

Synthesis and Characterization of Gold-Titanium-Mesoporous Silica Nanomaterials

Tay Shiau Fong*, Mohd Rafie Johan and Roslina Binti Ahmad

Advanced Materials Research Laboratory, Department of Mechanical Engineering, University of Malaya, 50603 Kuala Lumpur, Malaysia

*E-mail: nicotay@hotmail.com

Received: 15 February 2012 / Accepted: 4 April 2012 / Published: 1 May 2012

In situ process was used to prepare Au-Ti-mesoporous silica (MPS). The synthesized catalyst was characterized by a series of techniques such as, powder X-ray diffraction (XRD), transmission electron microscopy (TEM), nitrogen adsorption-desorption, thermogravimetry analysis (TGA), nitrogen adsorption desorption and UV-visible spectroscopy (UV-vis). XRD pattern showed the well organized of gold nanoparticles on Ti-mesoporous silica. Au-Ti-MPS which is eliminated via extraction with ethanol successfully maintains the typical wormhole structure of mesoporous silica and possess uniform mesoporous, spherical gold particle size (approximately 10nm) which is confirmed by TEM and nitrogen adsorption. UV-visible spectroscopy results confirm the simultaneous existence of Au and Ti active centre in this catalyst. Absorption peaks appear at wavelength of 220nm and 520nm. Optical band gap was obtained from the sample as well. The sensitivity of the optical properties of gold nanoparticles to agglomeration has been employed to detect low concentrations of heavy metal ions; Cu^{2+} and Zn^{2+} in water.

Keywords: In Situ; Mesoporous materials; electron microscopy; X-ray diffraction; Calcination

1. INTRODUCTION

Supported gold catalysts have been intensively studied in recent years [1]. As research goes forward, various supports and preparation methods have been developed. Gold catalysts were prepared by several methods, such as co-precipitation [2], deposition-precipitation (DP) [3], chemical vapor deposition [4], laser vaporisation [5], modified impregnation [6] and photo-deposition (PD) [7]. Examples like, Au-supported on MCM-41 was generated successfully by co-precipitation and incipient wetness impregnation [8]. Au-supported on Ti-SBA-15 was prepared by either grafting or direct synthesis [9].

Mesoporous materials are novel if compare to microporous and macroporous materials due to its capacious pore channels and large specific surface area. Titanium itself, even in nonporous structure, is a very useful functional material for several technologically demanding applications, including solar energy conversion [10–12], batteries and photocatalysis [13]. For example, titanium can be partially reduced and allows absorption of oxygen on the oxide surface for catalysis, which indeed makes it an excellent catalyst [1,14]. Moreover, due to the strong interactions with metal nanoparticles, such as Au, Ag and Pt, titanium has long been considered as a supporting matrix to prevent aggregation and thus improve the dispersibility of NPs [15-17]. These titanium-based nanocomposites have been proven to exhibit unique optical and electrical behaviour, including photoluminescence, surface Plasmon resonance (SPR), non-linear optical behaviour, and catalytic activities [18–21]. The unusual optical and chemical behaviour arises from the quantum size effects of NPs embedded in the host matrices and from the interactions at the interfaces over varying lengthy scales.

Gold exhibits a unique catalytic nature and action when it is deposited as nanoparticles on a variety of metal oxides. Currently, nano-sized gold materials are employed in CO gas sensors, low temperature CO oxidation in hydrogen stream, selective oxidation of alkanes, olefins and alcoholic compounds, etc [22-24]. The catalytic and adsorption properties are influenced by the dispersion, structure and interaction of gold nanoparticles with the support as well as by the support type [25]. Spherical gold nanoparticles are the most stable metal nanoparticles. They present fascinating aspects such as the behaviour of the individual particles, size-related electronic, magnetic and optical properties (quantum size effect), and their applications to catalysis and biology.

Applications of gold nanoparticles like sensors are usually based on detecting the shifts in surface Plasmon resonance (SPR) peak, due to either change in the dielectric constant around the nanoparticles as a result of adsorption of analyte molecules, or due to analyte-induced agglomeration of the nanoparticles.

In this work, we synthesize the gold nanoparticles supported on Ti modified mesoporous silica using in situ method and report the sensitivity of the optical properties of Au-Ti modified mesoporous silica to agglomeration have been employed to detect low concentration of heavy metal ions in water.

2. EXPERIMENTAL

Au-Ti-mesoporous silica was synthesized through an in situ process. First solution: 1.25 grams dodecylamine was added in the mixture of 14.3 grams de-ionized water and 7.6 grams ethanol while stirring. Meanwhile, 5.2 grams tetraethyl orthosilicate was added in the mixture of 1.55 grams isopropyl alcohol and 0.17 grams tetrabutyl orthotitanate as second solution. Second solution and 20 ml ethanol solution of HAuCl_4 (0.024 M) were simultaneously dropped into first solution then aged for 20 hours with vigorous stirring. The product solution was filtered and washed by de-ionized water, then dried at 333 K. The dried powder was calcined at 673 K and indicated as Au-Ti-MPS.

The absorption spectra of Au-Ti-MPS were measured by using a UVIKON 923 Double Beam UV-visible spectrophotometer and thermogravimetry analysis (TGA). Nitrogen adsorption isotherm was measured and the pore size distribution was calculated. Transmission electron microscopy (TEM) samples were prepared by placing a drop of dilute ethanol suspension of Au-Ti-modified MPS on the surface of a 300 mesh copper grid operating at 120kV. X-ray diffraction (XRD) analysis was carried out using a Siemens D500 X-ray diffractometer equipped with graphite monochromatized Cu K α radiation ($\lambda = 1.5418 \text{ \AA}$) irradiated with a scanning rate of $0.02^\circ \text{ s}^{-1}$. To demonstrate the detection of heavy metals, 0.01M Copper (II) sulfate and zinc acetate were prepared. The synthesized gold nanoparticles catalyst was exposed to various concentrations of Zn $^{2+}$ and Cu $^{2+}$ ions.

3. RESULTS AND DISCUSSION

3.1. XRD Studies

The XRD measurements were employed in order to study the mesoporous structure of the supports and calculation of gold particles size at calcination temperature, 673K. Figure 1 shows the wide-angle XRD-patterns of Au-Ti-MPS calcined at temperature of 673 K. The four Bragg reflections at 38.3° , 44.7° , 64.9° and 77.9° were assigned to the diffractions of (111), (200), (220) and (311) face-centered cubic structures. Intensity of the peaks reflects the order of gold particle size.

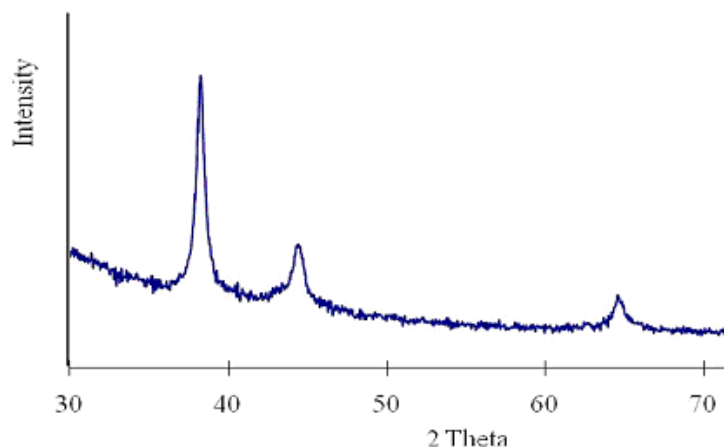


Figure 1. X-ray diffraction pattern of Au-Ti-MPS.

The crystallite size of gold can be deduced from XRD line broadening using the Debye-Scherrer equation [26]

$$L = \frac{\kappa\lambda}{\beta \cos\theta} \quad (1)$$

Where L is the crystallite size of gold, κ is a constant ($=0.9$), λ is the wavelength of X-ray ($\text{Cu K}\alpha = 1.5406 \text{ \AA}$), β is the true half-peak width, and θ is the half diffraction angle of the centroid of the peak in degree. The gold crystallite size calculated from the XRD peaks at $2\theta=38.3^\circ$ is 5.25nm .

Figure 2, represents low-angle powder XRD pattern of the sample. The sample exhibits a diffraction peak at 2.4° , which is a characteristic of mesoporous materials (MPS). [27]

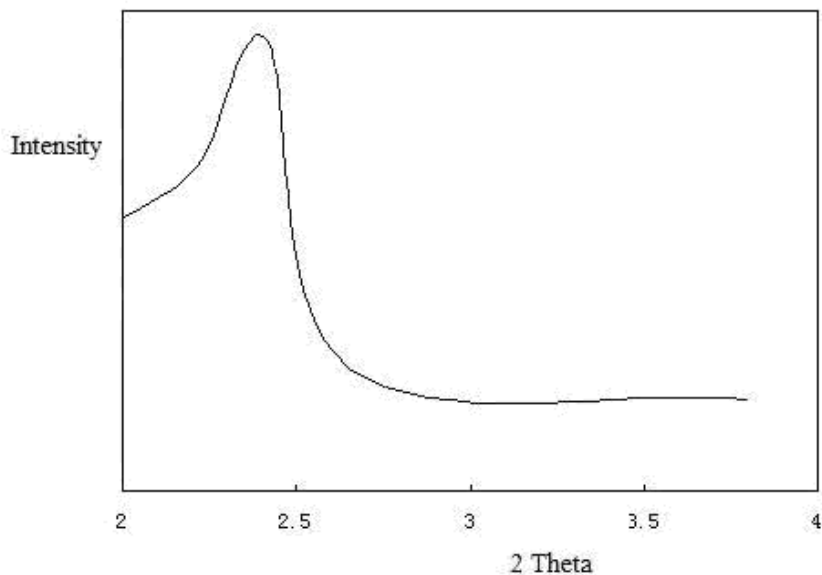


Figure 2. Low-angle X-ray diffraction pattern of Au-Ti-MPS.

3.2. TEM Studies

The TEM images shown in Figure 3 - 4 provide insights into the framework structure of Au-Ti-MPS. The spherical gold particles (black dots) are fairly distributed on the support surface.

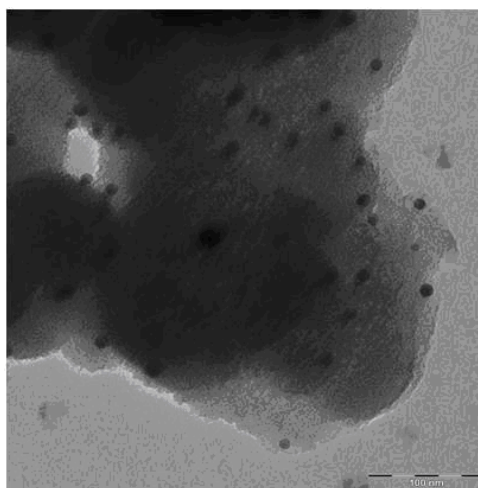


Figure 3. TEM image of Au-Ti-MPS.

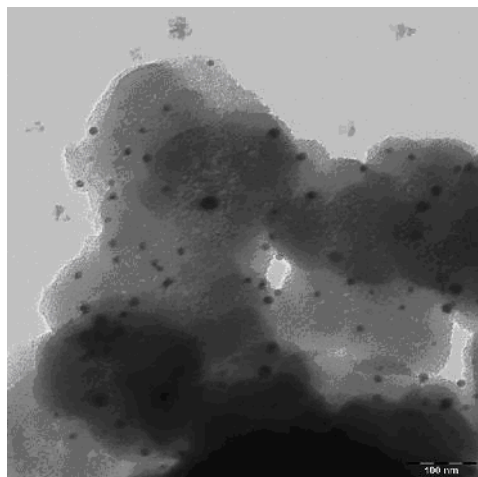


Figure 4. TEM image of Au-Ti-MPS.

The average particle sizes of gold were calculated to be 10.60 nm with a narrow particle size distribution as shown in Figure 5. It is shown that the gold particle size is smaller than 50nm size; thus, gold particles were successfully capped by mesoporous silica.

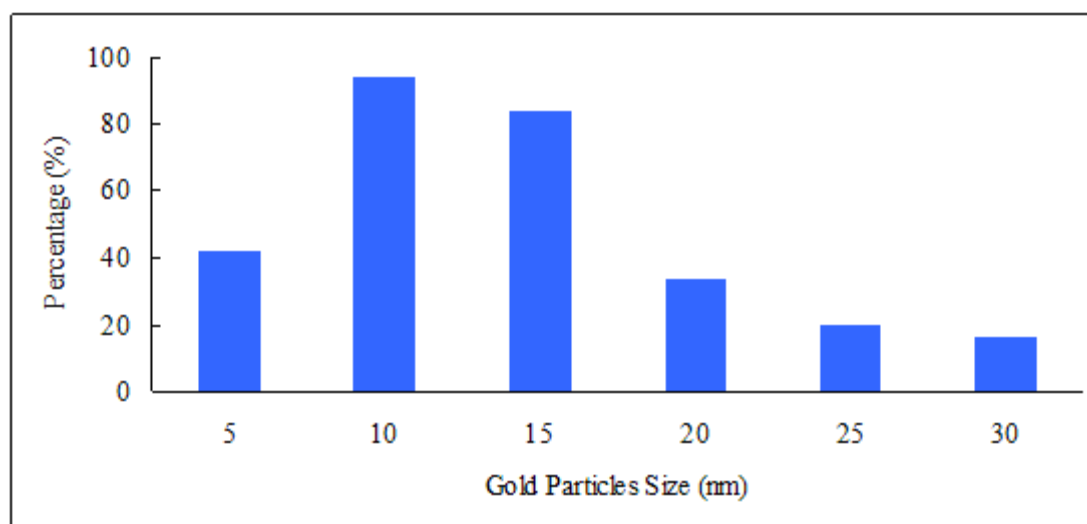


Figure 5. Particles size distribution of gold nanoparticles.

3.3. TGA

The purpose of TGA experiment is to determine the thermal stability of the sample. Figure 6 shows TGA curve of sample Au-Ti-MPS. The weight loss for sample occurs at around 100 °C. It is mainly due to evaporation of water from the samples.

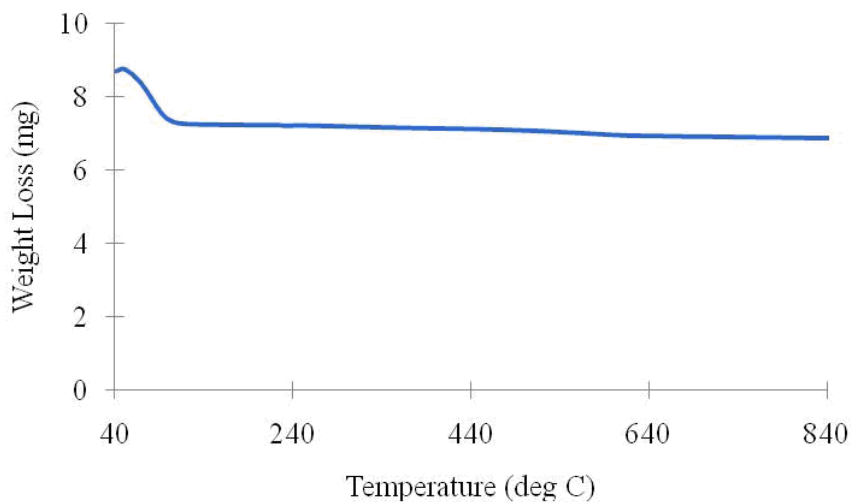


Figure 6. Thermogram of the Au-Ti-MPS.

3.4. Nitrogen Adsorption Desorption

Nitrogen adsorption measurements were performed to evaluate the quality and structural ordering of the synthesized materials. The nitrogen adsorption-desorption isotherm of the Au-Ti-MPS is shown in Figure 7. As seen from the Figure 7, Au-Ti-MPS exhibits type IV isotherm which is a typical H1 hysteresis loop typical of mesoporous solids. This type of hysteresis loop indicates that materials possess uniform pore size and shapes [28]. The position of relative pressure (P/P_0) at which the inflection steps are observed indicates pore diameter, whereas the sharpness of inflection gives information about pore uniformity. The sharp step at a relative pressure of 0.2-0.4 indicates the presence of framework-confined mesoporous with uniform dimension. From the Figure 8, the mean pore size of the sample is calculated, which is 2.1nm and the specific surface area is around 1018 m^2/g .

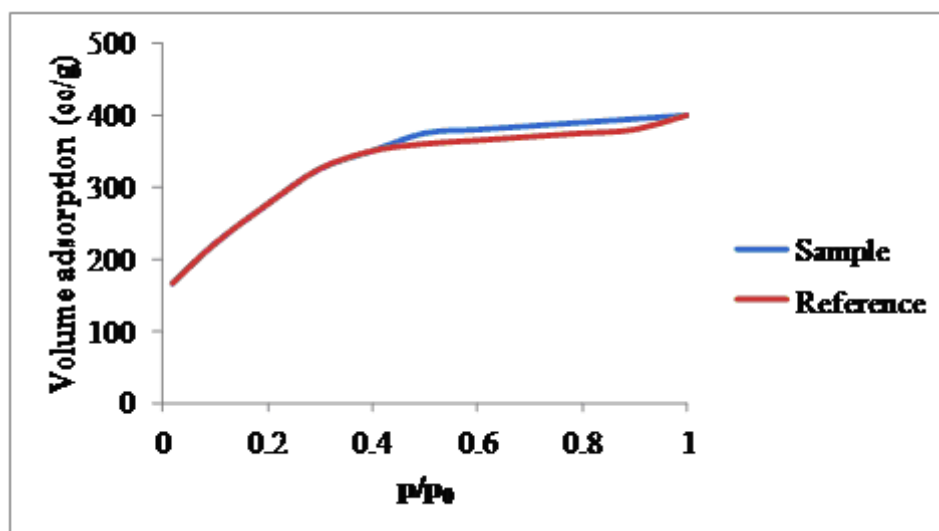


Figure 7. Nitrogen adsorption isotherm of the Au-Ti-MPS.

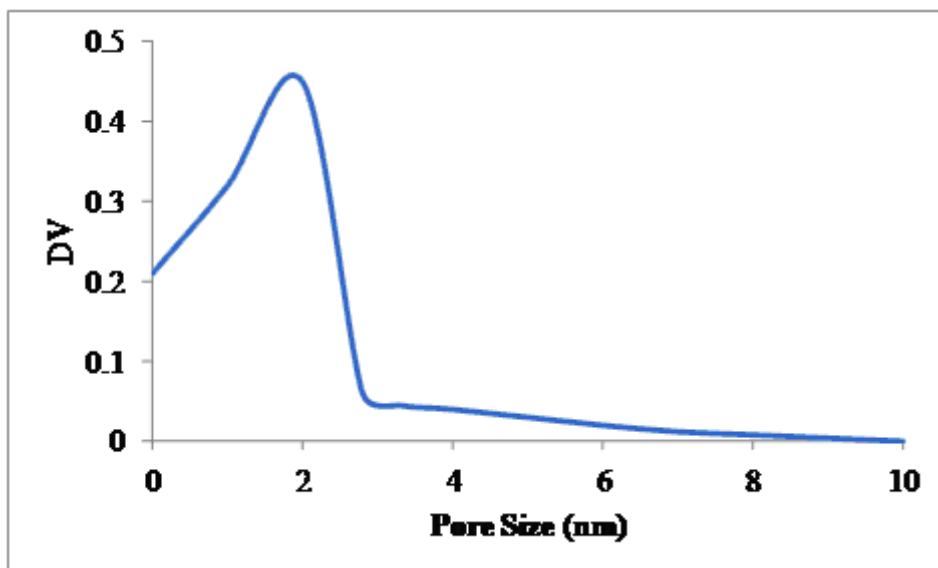


Figure 8. Pore size of Au-Ti-MPS.

3.5. UV-visible Studies

In Figure 9, the UV-visible spectrum of the Au-Ti-MPS is illustrated. The absorption band near 220 nm, which originates from the charge transfer of oxygen 2p electron to the empty 3d orbital of Ti^{4+} , indicates that framework Ti exists in tetrahedral coordination. The absorption band near 520 nm is assigned to the absorption of surface plasmon vibration in gold particles.

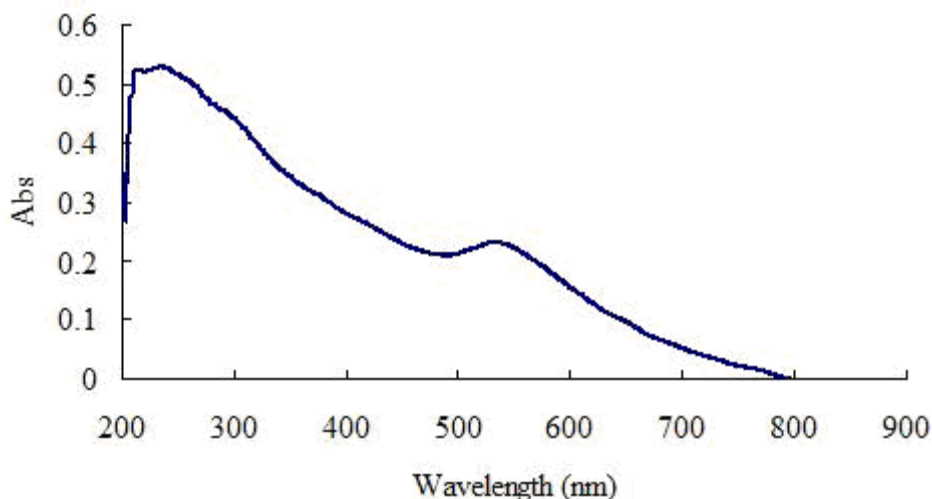


Figure 9. UV-visible absorbance spectrum of Au-Ti-MPS.

The reflectance spectrum recorded for the Au-Ti-MPS samples calcined at temperature 673K is shown in Figure 10. The band gap of the sample was determined by the equation:

$$E_g = \frac{1239.8}{\lambda} \quad (2)$$

Where E_g is the optical band gap (eV) and λ (nm) is the wavelength of the absorption edge in the spectrum [29]. The calculated band gap energy of the sample is 2.38eV, which is classified as semiconductor materials due to the gold nanoparticles were capped by mesoporous silica.

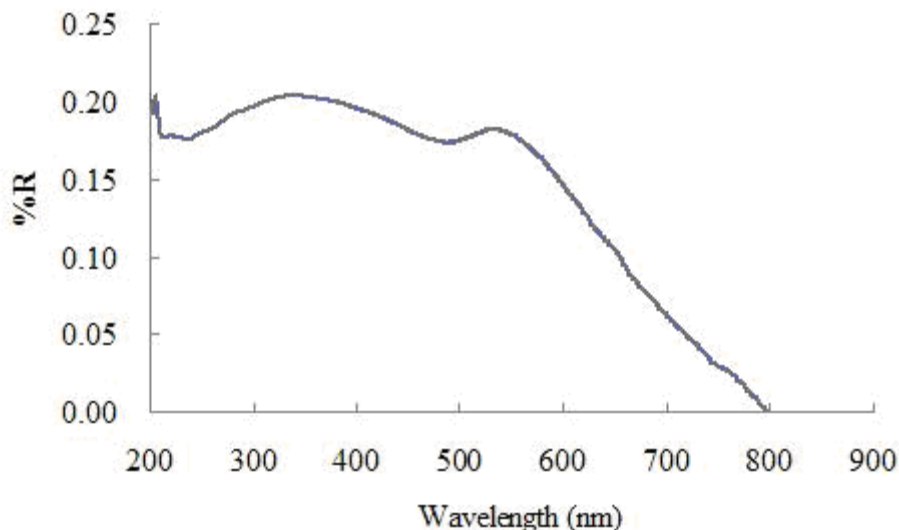


Figure 10. The reflectance spectrum of the samples.

Such colloidal suspensions are very sensitive to change in the concentration of ions in the solution. Addition of salts that change the ionic balance will result in loss of adsorbed anions from the nanoparticles, or exchange of the capping ions, resulting in agglomeration of the nanoparticles. As gold nanoparticles are no longer stabilized by physically adsorbed charges, upon exposure to varying concentration of these analytes, a concentration-dependant change in the optical absorption is observed (Figures 11 and 12). The width of the Plasmon resonance peak progressively increases with increase in concentration of Cu^{2+} and Zn^{2+} ions. The variation of the absorbance of light of 600nm wavelength with increased in concentration of both the analytes is plotted in Figures 13 and 14. The effect of capping the nanoparticles with Ti-MPS since it provides linear response with the increase in concentration of analytes. According from previous research paper on Chitosan-capped gold nanoparticles, effect of exposure to varying concentration of Cu^{2+} ions on their optical absorption spectra showed that the spectra shape for every sample is clearly distinguishable. However, the variation is not as uniform for Zn^{2+} ions. Thus, the comparison of changes in absorption value at 650nm due to varying Cu^{2+} ions was approximately linear response to chitosan-capped gold nanoparticles [30].

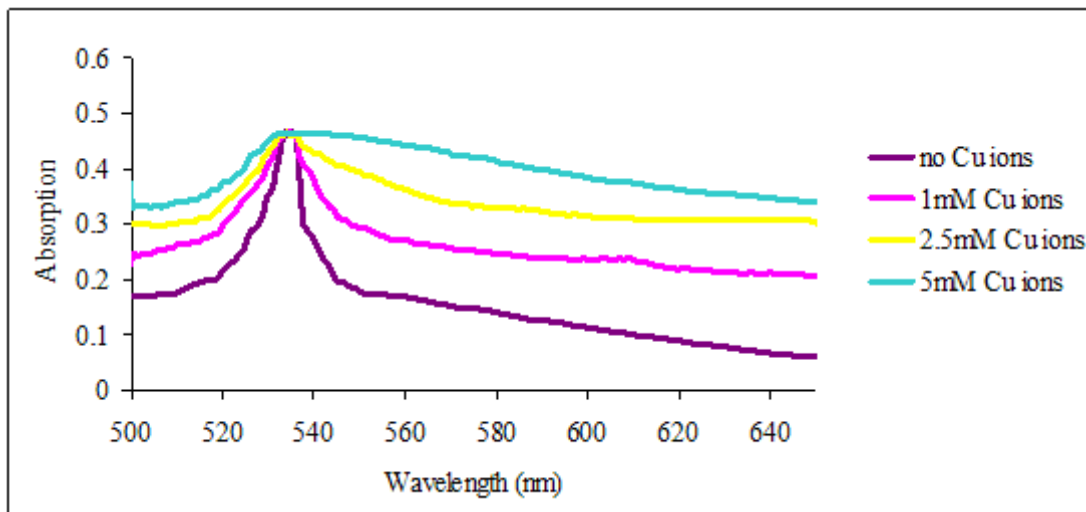


Figure 11. UV-visible absorbance spectra of Au-Ti-MPS on detecting Cu²⁺ ions.

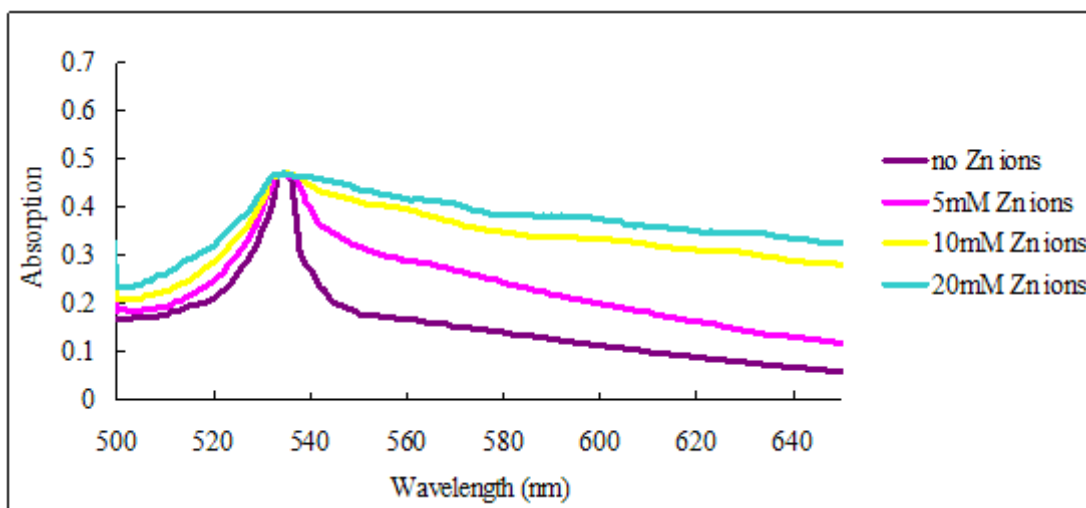


Figure 12. UV-visible absorbance spectra of Au-Ti-MPS on detecting Zn²⁺ ions.

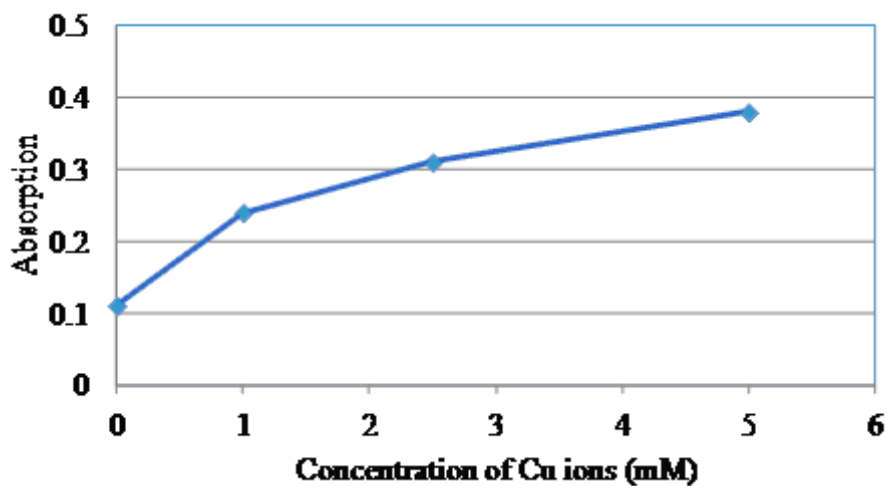


Figure 13. Comparison of optical absorption of 600nm light for varying concentration of Cu²⁺ ions.

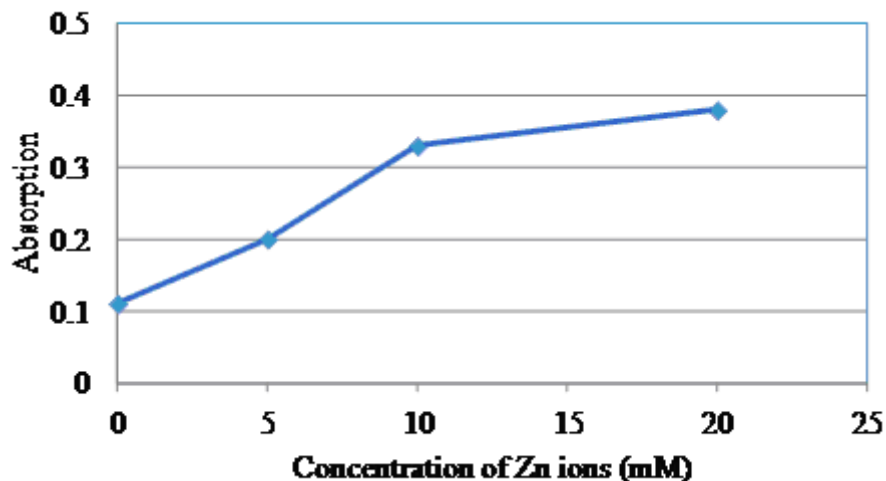


Figure 14. Comparison of optical absorption of 600nm light for varying concentration of Zn^{2+} ions.

4. CONCLUSION

Au-Ti-MPS nanoparticles were successfully produced via in situ method. The gold nanoparticles embedded in Ti-MPS were spherical in shape. From the results of XRD and TEM, the crystallite and physical sizes of the Au-Ti-MPS nanoparticles are less than 20 nm. The average physical size for Au-Ti-MPS is 10.6 nm. UV-visible spectroscopy results confirm the simultaneous existence of Au and Ti active centre in this catalyst. Absorption peaks appear at wavelength 220nm and 520nm. From UV-vis spectroscopy spectra, the band gap energy is calculated, 2.38eV. To demonstrate the detection of low concentration levels of heavy metal ions like Cu^{2+} and Zn^{2+} , a simple characterization tool like UV-visible adsorption spectrum is found to be sufficient to observe the concentration levels of the analyte. From the results, it is shown that the Au-Ti-MPS can be used to detecting existence of both Cu^{2+} and Zn^{2+} ions.

ACKNOWLEDGEMENTS

The authors acknowledge the support from the Institute Postgraduate Research Fund (PS097/2009C) to this work.

References

1. M. Schuber, S. Hackenberg, A.C. Veen, M. Muhler, V. Plzak and R.J. Behm, *J. Catalysis*, 197 (2001) 113.
2. M. Haruta, N. Yamada, T. Kobayashi, S. Iijima, *Journal of Catalysis*, 115 (1989) 301.
3. F. Moreau, G.C. Bond, A.O. Taylor, *J Catal* 231 (2005) 105.
4. M. Okumura, S. Nakamura, S. Tsubota, T. Nakamura, M. Azuma, M. Haruta, *Catal Lett* 51 (1998) 53.
5. C. Rossignol, S. Arrii, F. Morfin, L. Piccolo, V. Caps, J.L. Rousset, *J Catal*, 230, (2005) 476.
6. W.C. Li, M. Comotti, F. Schuth, *J Catal* 237 (2006) 190.

7. G.R. Bamwenda, S. Tsubota, T. Nakamura, M. Haruta, *Catal Lett* 44 (1997) 83
8. L.Sobczak, A. Kusior, J. Grams, M.Ziolek, *J.Catal.* 245 (2007) 259-266.
9. E.Sacaliuc, A.M.Beale, B.M. Weckhuysen, T.A.Nijhuis, *J.Catal.* 248(2007)235-248
10. M. Gratzel, *Curr. Opin. Colloid* 4 (1999) 314.
11. M. Gratzel, *Prog. Photovolt. Res. Appl.* 8 (2000) 171.
12. A. Hagfeldt, M. Gratzel, *Acc. Chem. Res.* 33 (2000) 269.
13. M.R. Hoffmann, S.T. Martin, W.Y. Choi, D.W. Bahnemann, *Chem. Rev.* 95 (1995) 69.
14. B.M. Yang, M. Kalwei, F. Schuth, K.J. Chao, *Appl. Catal. A – Gen.*254 (2003) 289.
15. P. Claus , A. Bruckner, C. Mohr, H. Hofmeister *J. Am. Chem. Soc.* 122 (2000) 11430
16. M. Jakob, H. Levanon, P.V. Kamat *Nano Lett.* 3 (2003) 353.
17. M.S. Chen, D.W. Goodman, *Science* 306 (2004) 252.
18. N. Chandrasekharan, P.V. Kamat, *J. Phys. Chem. B* 104 (2000) 10851.
19. L. Armelao, D. Barreca, G. Bottaro, A. Gasparotto, E. Tondello, M. Ferroni, S. Polizzi, *Chem. Mater.* 16 (2004) 3331.
20. J. Chou, E.W. McFarland, *Chem. Comm.* (2004) 1648.
21. D. Li, J.T. McCann, M. Gratt, Y.N. Xia, *Chem. Phys. Lett.* 394 (2004) 387.
22. T.Kobayashi, M.Haruta, S.Tsubota, H. Sano, *Sens. Actuators B1* (1990) 222
23. V.V. Gorodetskii, W. Drachsel, *Applied Catalyst A:Gen.* 188(1999) 267.
24. V.P. Zhdanov, B. Kasemo, *Surface Science Letter* 511 (2002) 23.
25. M. Brust, M. Walker, M. Bethell, D. Schiffrin, R. Whyman, *J. Chem. Soc. Chem. Commun* (1994) 801.
26. B.D. Cullity, *Elements of X-ray diffraction*, Addison-Wesley Pub, Notre Dame (1978).
27. P.T.Tanev, M.Chibwe, T.J.Pinnavaia, *Nature* 368 (1994)321
28. T.A. Zepeda, J.I.G. Fierro, B. Pawelec, R. Nava, A. Montesinos, A. Olivas, S. Fuentes, T. Halachev, *Chemistry Material.* 17 (2005)4062.
29. B. Oregan, M. Gratezl, *Nature* 353 (1991) 737.
30. A.Sugunan, C.Thanachayanont, J. Dutta, J.G. Hilborn, *Science and Technology of Advanced Materials* 6 (2005) 335-340.